recent results of Engel *et al.* on the Fenna-Matthew-Olson complex of green sulfur bacteria also suggest strong correlations between the fluctuations of the neighboring one-exciton states of the complex (*4*). Clearly, further studies are required before it can be stated that correlated fluctuations and the consequent protection of electronic coherence is a general feature of photosynthetic pigment-protein complexes, but it seems clear that any accurate description of the dynamics (and design principles) of these systems will require proper consideration of both quantum coherences and long-range system-bath interactions (*3*, *22*, *23*).

We close by briefly comparing the present technique with existing experimental methods. In principle, 2D electronic spectroscopy (*4*, *28*, *29*) and pump-probe anisotropy spectroscopy (*10*, *23*, *30*) both contain information about coherence dynamics in the form of quantum beatings. However, interferences from other coherence states and population relaxation can create a complicated beating pattern that makes a quantitative analysis of coherence dynamics in the 2D spectrum or an anisotropy decay difficult. In this regard, the 2CECPE technique provides a unique tool that can resonantly select third-order response contributions from a specific coherence pathway and should lead to a much-improved understanding of coherence dynamics and the protein fluctuations that govern these dynamics.

References and Notes

1. R. E. Blankenship, *Molecular Mechanisms of Photosynthesis* (Blackwell Science, Oxford, 2002).
2. R. van Grondelle, V. I. Novoderezhkin, *Phys. Chem. Chem. Phys.* **8**, 793 (2006).
3. O. Kühn, V. Sundström, T. Pullerits, *Chem. Phys.* **275**, 15 (2002).
4. G. S. Engel *et al.*, *Nature* **446**, 782 (2007).
5. U. Ermler, G. Fritzsch, S. K. Buchanan, H. Michel, *Structure* **2**, 925 (1994).
6. C. A. Wraight, R. K. Clayton, *Biochim. Biophys. Acta* **333**, 246 (1973).
7. R. J. Stanley, B. King, S. G. Boxer, *J. Phys. Chem.* **100**, 12052 (1996).
8. J. A. Jackson *et al.*, *J. Phys. Chem. B* **101**, 5747 (1997).
9. M. H. Vos, J. Breton, J.-L. Martin, *J. Phys. Chem. B* **101**, 9820 (1997).
10. D. C. Arnett, C. C. Moser, P. L. Dutton, N. F. Scherer, *J. Phys. Chem. B* **103**, 2014 (1999).
11. Materials and methods are available as supporting material on *Science* Online.
12. R. Agarwal, B. S. Prall, A. H. Rizvi, M. Yang, G. R. Fleming, *J. Chem. Phys.* **116**, 6243 (2002).
13. M. A. Rickard, A. V. Pakoulev, K. Kornau, N. A. Mathew, J. C. Wright, *J. Phys. Chem. A* **110**, 11384 (2006).
14. I. V. Rubtsov, J. Wang, R. M. Hochstrasser, *Proc. Natl. Acad. Sci. U.S.A.* **100**, 5601 (2003).
15. S. J. Jang, M. D. Newton, R. J. Silbey, *Phys. Rev. Lett.* **92**, 218301 (2004).
16. T. Meier, V. Chernyak, S. Mukamel, *J. Chem. Phys.* **107**, 8759 (1997).
17. M. L. Groot, J. Y. Yu, R. Agarwal, J. R. Norris, G. R. Fleming, *J. Phys. Chem. B* **102**, 5923 (1998).
18. X. J. Jordanides, G. D. Scholes, W. A. Shapley, J. R. Reimers, G. R. Fleming, *J. Phys. Chem. B* **108**, 1753 (2004).
19. D. Y. Parkinson, H. Lee, G. R. Fleming, *J. Phys. Chem. B* 10.1021/jp070029q (2007).
20. We used $\lambda_h = 50\ cm^{-1}$, $\lambda_b = 80\ cm^{-1}$, $\tau_h = \tau_b = 60$ fs, and $\Delta_h = \Delta_b = 20\ cm^{-1}$, and we assumed the electronic coupling $J = 220\ cm^{-1}$ and the gap between excitonic H and B states is $680\ cm^{-1}$; these values are well within the range suggested by other theoretical studies and our recent experiments (*16*–*19*).
21. M. Souaille, M. Marchi, *J. Am. Chem. Soc.* **119**, 3948 (1997).
22. T. Renger, V. May, O. Kühn, *Phys. Rep.* **343**, 137 (2001).
23. V. Novoderezhkin, M. Wendling, R. van Grondelle, *J. Phys. Chem. B* **107**, 11534 (2003).
24. H. Treutlein *et al.*, *Proc. Natl. Acad. Sci. U.S.A.* **89**, 75 (1992).
25. P. de Bree, D. A. Wiersma, *J. Chem. Phys.* **70**, 790 (1979).
26. Y. Ohtsuki, Y. Fujimura, *J. Chem. Phys.* **91**, 3903 (1989).
27. J. M. Jean, G. R. Fleming, *J. Chem. Phys.* **103**, 2092 (1995).
28. T. Brixner, T. Mančal, I. V. Stiopkin, G. R. Fleming, *J. Chem. Phys.* **121**, 4221 (2004).
29. A. V. Pisliakov, T. Mančal, G. R. Fleming, *J. Chem. Phys.* **124**, 234505 (2006).
30. K. Wynne, R. M. Hochstrasser, *Chem. Phys.* **171**, 179 (1993).

31. This work was supported by the Office of Basic Energy Sciences, Chemical Sciences Division, U.S. Department of Energy (contract DE-AC03-76SF000098). We thank S. G. Boxer for *R. sphaeroides* samples; B. S. Prall and D. Y. Parkinson for valuable discussions; and E. A. Berry, L. S. Huang, and N. G. Pon for help with sample preparation.

Supporting Online Material

www.sciencemag.org/cgi/content/full/316/5830/1462/DC1
Materials and Methods
Figs. S1 to S2
References

6 March 2007; accepted 26 April 2007
10.1126/science.1142188

Stepwise Quenching of Exciton Fluorescence in Carbon Nanotubes by Single-Molecule Reactions

Laurent Cognet,[1,2]* Dmitri A. Tsyboulski,[2]† John-David R. Rocha,[2]† Condell D. Doyle,[2] James M. Tour,[2] R. Bruce Weisman[2]*

Single-molecule chemical reactions with individual single-walled carbon nanotubes were observed through near-infrared photoluminescence microscopy. The emission intensity within distinct submicrometer segments of single nanotubes changed in discrete steps after exposure to acid, base, or diazonium reactants. The steps were uncorrelated in space and time and reflected the quenching of mobile excitons at localized sites of reversible or irreversible chemical attack. Analysis of step amplitudes revealed an exciton diffusional range of about 90 nanometers, independent of nanotube structure. Each exciton visited about 10,000 atomic sites during its lifetime, providing highly efficient sensing of local chemical and physical perturbations.

Optical excitation of semiconducting single-walled carbon nanotubes (SWNTs) generates relatively strongly bound excitons whose spatial dimensions are predicted to be a few nanometers (*1*–*3*). Experimental evidence of efficient exciton-exciton annihilation in nanotubes indicates that SWNT excitons have substantial mobility along the tube axis (*4*–*6*). However, the extent of this mobility is still experimentally and theoretically uncertain. A notable related effect is the strong suppression of photoluminescence (PL) when SWNT sidewalls are perturbed by chemical reactions (*7*–*9*). This quenching phenomenon has hampered the use of covalently derivatized SWNTs as near-infrared (near-IR) fluorophores.

We report the use of single-nanotube microscopy to detect stepwise changes in SWNT PL intensity within segments of individual nanotubes while they are exposed to chemical reactants. These stepwise changes in PL intensity are caused by reactions of single molecules with one nanotube. Since the pioneering low-temperature experiments of Orrit and Moerner, single-molecule spectroscopy has proven to be a powerful tool that bypasses ensemble averaging in the study of static and dynamic nano-objects in various environments (*10*, *11*). Single-molecule approaches are especially appealing for SWNT fundamental studies and applications (*12*–*14*) because the bulk samples are highly heterogeneous. In the present work, the magnitudes of PL intensity steps caused by single-molecule reactions reveals that the exciton excursion range in highly luminescent SWNTs is ~90 nm and is essentially independent of nanotube structure. This room-temperature excitonic motion is deduced to be diffusional. Because each nanotube exciton visits a very large number of atomic sites during its lifetime, PL quenching provides an ultrasensitive method for sensing and studying certain types of chemical reactions with nanotube sidewalls at the single-molecule level.

Our studies required highly luminescent and relatively long nanotubes that were immobilized yet accessible to added reactant solutions. We therefore used very brief tip ultrasonication to

[1]Centre de Physique Moléculaire Optique et Hertzienne, Université Bordeaux 1, and CNRS, Talence F-33405, France. [2]Department of Chemistry, Center for Biological and Environmental Nanotechnology, and R. E. Smalley Institute for Nanoscale Science and Technology, Rice University, Houston, TX 77005, USA.

*To whom correspondence should be addressed. E-mail: lcognet@u-bordeaux1.fr (L.C.); weisman@rice.edu (R.B.W.)
†These authors contributed equally to this work.

disperse raw high-pressure CO (HiPco) SWNTs in aqueous sodium dodecylbenzenesulfonate (SDBS) surfactant before mixing the dilute suspension with a melted agarose gel preparation (*15*). Aqueous gels are commonly used in molecular biology to provide an inert immobilizing environment and have previously been applied in single-molecule optical measurements (*16*). We captured near-IR fluorescence images of single nanotubes with a wide-field inverted microscope modified to include laser excitation and a low-noise InGaAs camera (*14*). Individual SWNTs a few micrometers in length were easily identified in these images, and some of them displayed uniform and high PL intensity (Fig. 1A). The (*n*,*m*) structural assignment of each studied tube was deduced from the peak wavelength of its narrow Lorentzian emission spectrum (*17*), as measured with a dedicated spectrograph and multichannel near-IR detector (Fig. 1B). In this study, we selected the brightest nanotubes present in the weakly sonicated samples. We believe that these selected nanotubes have low defect densities and nonradiative relaxation rates that are dominated by intrinsic processes. Most of these nanotubes displayed PL that varied linearly at the excitation intensities used here and remained stable for tens of minutes under continuous illumination (Fig. 1, B and C). We used low laser intensities (~100 W/cm^2) to avoid exciton-exciton annihilation effects that would shorten the exciton lifetime and reduce the exciton's excursion range (*4*–*7*). Furthermore, we verified that the nanotubes studied here showed no detectable spectral shifts, spectral broadening, or change in emission intensity during the typical duration of our experiments (Fig. 1B). Finally, we confirmed that the emission spectra of SWNTs embedded in agarose gels matched those of SWNTs in fluid surfactant suspension.

To initiate chemical reactions, we placed a 10-μl drop of reactant solution on the edge of the 20 mm by 20 mm sample gel while recording fluorescence images of a specific nanotube with stable and spatially uniform emission (fig. S1). Two reactants were used. One was sulfuric acid (0.05 M), which causes pH-dependent, reversible quenching of SWNT fluorescence (*7*, *8*, *18*). The other was 4-chlorobenzenediazonium tetrafluoroborate (1 mg/ml in water), which is known to give irreversible covalent derivatization of carbon atoms on the nanotube sidewall (*19*). We recorded fluorescence image sequences at an 18-Hz frame rate and plotted the total intensity within selected 2 × 2 pixel regions to obtain PL intensity traces. The chosen spatial binning region (4 pixels) corresponded to 670 nm by 670 nm, which is essentially the diffraction limit at the near-IR wavelengths.

The PL intensity trace from a 670-nm segment of an individual (8,6) nanotube after exposure to sulfuric acid is shown in Fig. 2A. That nanotube's luminescence spectrum is plotted in Fig. 2B. Coarsely, the PL time trace displays an exponential decay form. However, closer examination reveals a series of strikingly distinct steps between well-defined intensity levels, rather than a continuous decrease (Fig. 2A, inset). Moreover, the luminescence shows upward as well as downward steps. To analyze the distribution of step amplitudes, we compiled a histogram for the first 108-s period, showing signal differences (δI) between successive image frames (Fig. 2C). Apart from the large main peak near zero, whose width arises mainly from signal noise, there are four distinct side bands distributed symmetrically around zero. These side bands are the signature of specific step amplitudes. The inner two (labeled +1 and –1) correspond to positive and negative steps of the same unit intensity, whereas the outer two (+2 and –2) correspond to double-amplitude steps. The presence of discrete (quantized) intensity changes is confirmed by the precisely linear relation linking the amplitudes of these intensity steps (Fig. 2D).

We attribute the observed discrete intensity steps to individual protonation reactions at the nanotube surface. The –1 and –2 steps would arise, respectively, from one or two independent sidewall reactions occurring within the 54-ms sampling interval, whereas the +1 and +2 steps would arise from the reverse chemical processes. The mechanism through which acids quench nanotube luminescence has been described as a protonation at the sidewall of the nanotubes (*7*, *8*, *18*). In this scheme, a hole is injected into the nanotube π-system near the protonation site. If an exciton encounters such a chemically induced hole before it radiatively recombines, the exciton's luminescence will be efficiently quenched through nonradiative Auger processes (*6*).

Because the excitons have a limited excursion range, only a fraction of those generated within an observed 670-nm segment will be quenched by a single protonation-induced hole. If the density of such holes is low, then each one causes the

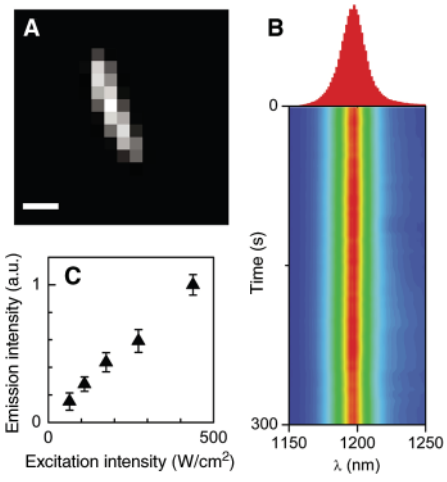

Fig. 1. Fluorescence measurements on an individual SWNT immobilized in agarose gel. (**A**) Image of an (11,3) SWNT excited at 100 W/cm^2. Scale bar, 1 μm; the intensity scale is linear from 0 (black) to 45,000 camera counts (white). (**B**) Spectrum of the same nanotube (top) and color-coded contour plot (bottom) showing the stability of spectra taken at 5-s intervals for 300 s. (**C**) Luminescence intensity from the same nanotube as a function of excitation intensity. Linearity up to 500 W/cm^2 indicates that no multiexciton processes occur at 100 W/cm^2, which is the excitation intensity used in this study.

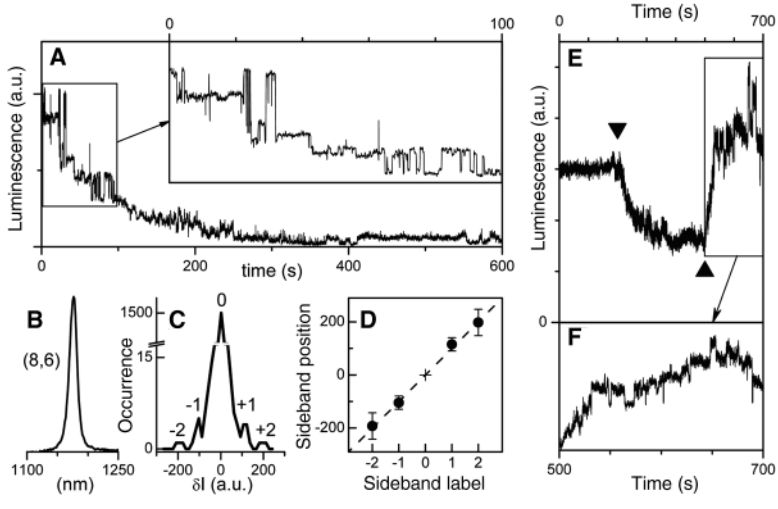

Fig. 2. Reversible stepwise quenching of individual SWNTs by acid. (**A**) Luminescence intensity of a diffraction-limited segment of an individual (8,6) SWNT after addition of acid. Inset shows an expansion of the first 100-s period, revealing well-defined reversible steps. (**B**) Near-IR emission spectrum of this SWNT, showing a single Lorentzian peak. (**C**) Histogram constructed from the data in the inset of (A), showing the distribution of changes in luminescence signal (δI) between successive 50-ms frames. Four symmetrically located side bands are evident at well-defined δI values. (**D**) Sideband peak positions as a function of sideband label. The linear relationship indicates that the side bands correspond to discrete protonation and deprotonation steps (see text). (**E**) Luminescence signal of a diffraction-limited segment of an individual (7,6) SWNT upon successive addition of acid (▼) and base (▲). Luminescence recovery is observed after base addition. (**F**) Expanded inset from (E) showing reversible steps in the recovery period.

same amount of quenching (corresponding to the observed –1 step amplitude), and each deprotonation restores the same amount of luminescence (the observed +1 step amplitude). However, when the typical distance between quenching sites becomes shorter or comparable to the exciton excursion range, the quenching impact of additional sites is reduced, giving smaller and eventually unresolved steps, as seen at later times in Fig. 2A.

To confirm that the observed stochastic stepwise quenching arises from reversible protonation, we added ~10 μl of 1 M NaOH to nanotube samples that had previously been quenched by acid addition. The inverted triangle in Fig. 2E marks the point of acid addition, and the standard triangle marks the point of base addition. The period of luminescence restoration is expanded in Fig. 2F, which shows the expected stochastic stepwise intensity changes. Statistical analysis of upward and downward steps in a medium of known pH can in principle provide the pK_a of the protonated nanotube. However, we could not perform this analysis on our data because of time-dependent pH gradients in the sample. Large intensity fluctuations were observed after luminescence was restored by base addition. We attribute this behavior to local pH fluctuations near the nanotube within the agarose pores after the successive addition of acid and base without active mixing. Finally, the higher intensities seen in Fig. 2E after restoration likely reflect a higher final pH level at the nanotube (*18*).

To compare these exciton-quenching effects with those caused by an irreversible chemical reaction, we performed similar measurements on samples exposed to diazonium salts (Fig. 3) (*20*). These traces also display distinct steps in luminescence intensity, but the great majority of the steps are negative (>95%), indicating a mainly irreversible process (*9*). Adjacent diffraction-limited segments within a single nanotube exhibited very different dynamics, with little or no correlation between the time positions of the steps (compare each set of red and black traces in Fig. 3, A to C). Similar spatially uncorrelated behavior in acid quenching is vividly illustrated in movie S1. This observation demonstrates that the mean excursion range of excitons must be smaller than our optical resolution of 670 nm. The same conclusion can be drawn from the localized PL in bent nanotubes excited by linearly polarized light (*14*) (fig. S2).

Comparison of the PL time traces within each frame of Fig. 3, A to C, reveals that for different segments of one nanotube, the first few step heights are integer multiples of the same unit intensity change Δ (regions marked by single asterisks). This stepwise quenching pattern leads to emission intensity plateaus that match between distinct segments of the same tube. As was observed for acid quenching, the steps have identical amplitudes at low densities of quenching sites, and they have gradually smaller amplitudes at longer times when the typical distance between quenching sites becomes shorter than or comparable to the exciton excursion range. However, in contrast to the reversible protonation reaction of acid quenching, the single-molecule diazonium salt reactions are essentially irreversible. Here, the chlorobenzenediazonium ion (or its diazotate dimeric product) is thought to first adsorb onto the surface of a nanotube, forming a charge transfer complex. The complex then irreversibly decomposes to form a covalent bond with the nanotube surface (*9*, *21*).

We presume that either of these nanotube perturbations can cause efficient exciton nonradiative decay. A mechanism for luminescence quenching by sidewall derivatization is suggested by scanning tunneling spectroscopy results on nanotubes covalently functionalized with amido groups, obtained with 10-nm resolution. The semiconducting energy gap was locally filled at the derivatization site (*22*). Excitons encountering such electronic perturbations should undergo efficient nonradiative recombination.

For each nanotube studied, repeatable values of Δ are obtained at early stages of the reaction when only a few independent sites have been derivatized within the observed diffraction-limited segment. We found that Δ values matched for separate segments in a single nanotube (Fig. 3, A to C). As for the minor variations in intensity step heights found at early stages of the reaction, we attribute these to the finite length of the diffraction-limited segment, because quenching events near the edge of the region produce smaller steps. Several simultaneous steps sometimes occurred within a single 54-ms frame (Fig. 3, A and B). This behavior probably results from nonuniform dilution of reactants in the submicrometer pores of the agarose gels, exposing the nanotube segments to large local concentration fluctuations.

Normalizing Δ by the initial luminescence intensity I gives a ratio representing the probability that a mobile exciton within the nanotube segment encounters a chemical reaction site during its lifetime. This probability also represents the fraction of the nanotube length explored by an exciton. The average exciton excursion range Λ is therefore simply given by $(\Delta/I) \times L$, where L is the observed segment length. For L = 670 nm, we measured Λ values for 19 different highly luminescent SWNTs. The resulting distribution is strikingly narrow, with a mean value of 91 nm (Fig. 4A). The small dispersion found for Λ values suggests that Λ does not depend strongly on nanotube structure. We plotted Λ values measured for 11 different (n,m) species (*23*) as a function of SWNT diameter (Fig. 4B) and found no systematic variation of exciton excursion range with diameter (for the range studied, 0.7 to 1.1 nm) or with chiral angle.

As mentioned above, our determination of Λ assumes that the local perturbation induced by a reaction sufficiently modifies the electronic structure of these bright tubes (*22*) to completely quench excitons at that site. If this quenching probability P is in fact less than 1, then Λ would be given by 90 nm/P (but could not exceed 670 nm). However, several observations support the estimate of P = 1. The results are independent of nanotube structure, the normalized initial step

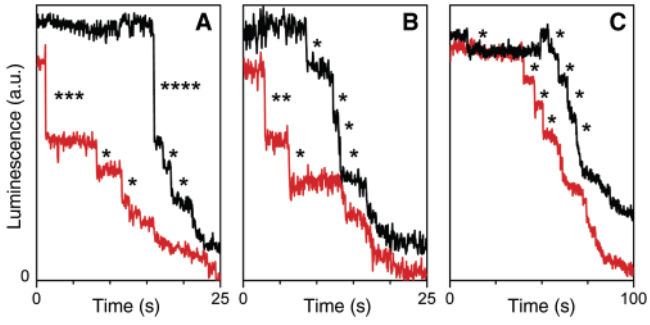

Fig. 3. Irreversible localized quenching of individual SWNTs with 4-chlorobenzenediazonium tetrafluoroborate. Luminescence quenching of diffraction-limited segments of individual SWNTs is shown for (8,3) (**A**), (8,6) (**B**), and (11,1) (**C**) species upon addition of the diazonium salt solution. Irreversible intensity steps are observed. Each asterisk marks an elementary unit step. In each frame, the red (lower) and black (upper) traces correspond to adjacent segments (each 670 nm in length) of the same nanotube. The black traces have been shifted upward by one unit step for clarity.

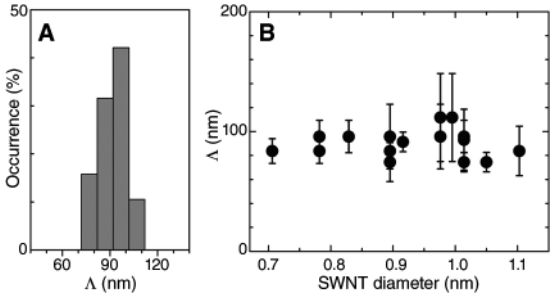

Fig. 4. Exciton excursion range (Λ) measured for various SWNTs. (**A**) Distribution (n = 19) of Λ values deduced from elementary step amplitudes (see text). (**B**) Plot of Λ values as a function of SWNT diameter.

amplitudes are consistent for acid quenching and diazonium salt quenching, and Auger quenching of excitons is known to be efficient.

Is the exciton motion ballistic or diffusional? For the bright emissive SWNTs studied here, we assume an exciton recombination lifetime τ = 100 ps, which is among the larger values reported from time-resolved spectroscopy (*24*, *25*), If the motion is ballistic, then the exciton's kinetic energy would be given by

$$E_{\text{ballistic}} = \frac{1}{2} m^*_{\text{exciton}} \left(\frac{\Lambda}{\tau}\right)^2 \quad (1)$$

where m^*_{exciton} is the exciton effective mass. Using an estimated m^*_{exciton} of ~$0.1m_e$ (*1*, *26*), we obtain $E_{\text{ballistic}} \sim 10^{-7}$ eV. This value is orders of magnitude lower than the 0.012 eV ($\frac{1}{2}k_BT$) expected from rapid thermalization induced by the exciton-phonon coupling evident in SWNT spectroscopy (*27*). We conclude that the excitonic motion is instead diffusional, in agreement with a recent investigation on bulk samples (*28*). The corresponding diffusion coefficient for the exciton one-dimensional random walk is then given as $D = \Lambda^2/2\tau \sim 0.4$ cm^2 s^{-1}.

This value lies more than two orders of magnitude below a prior tentative estimate that was indirectly deduced from transient absorption experiments on ensembles of short SWNTs in annealed dried films (*29*). The exciton diffusion coefficient measured here for highly luminescent individual SWNTs may be used to interpret the ~150 cm^{-1} Lorentzian line widths observed in emission spectroscopy of room-temperature SWNTs (see Figs. 1B and 2B). These widths arise from dephasing that is far more rapid (70 fs) than the ~100-ps exciton population lifetime τ.

If dephasing instead occurs by diffusional hopping of the exciton along the tube axis, then the hopping step length d_{hop} can be estimated from the relation $D = d_{\text{hop}}^2/2\tau_{\text{hop}}$, where τ_{hop} represents the interval between hops, identified as the 70-fs dephasing time. This approach gives a hopping step length of ~2 nm, which closely matches theoretical estimates of the exciton size (*1*–*3*). We propose that the emission linewidth may originate from thermally assisted short-range hopping of excitons along the nanotube axis. At cryogenic temperatures, suppression of this hopping would then remove the major source of line broadening and would account for markedly narrower spectral features (*30*).

If efficient exciton quenching occurs not only at chemical derivatization sites but also at the ends of cut nanotubes, our value of the exciton diffusion range Λ naturally explains the strong reduction in PL reported for SWNTs shorter than ~100 nm (*31*). More generally, the measured diffusion range implies that one exciton will visit ~10^4 carbon atoms during its lifetime. Thus, PL becomes remarkably sensitive to certain sidewall electronic perturbations, which may include chemical derivatizations and defects introduced during nanotube processing. PL may then prove useful for detecting local pH gradients in restricted environments, such as microfluidic channels or organelles inside biological cells.

References and Notes

1. T. G. Pedersen, *Phys. Rev. B* **67**, 073401 (2003).
2. V. Perebeinos, J. Tersoff, Ph. Avouris, *Phys. Rev. Lett.* **92**, 257402 (2004).
3. C. D. Spataru *et al.*, *Phys. Rev. Lett.* **92**, 077402 (2004).
4. J. Chen *et al.*, *Science* **310**, 1171 (2005).
5. Y.-Z. Ma *et al.*, *Phys. Rev. Lett.* **94**, 157402 (2005).
6. F. Wang *et al.*, *Phys. Rev. B* **70**, 241403R (2004).
7. M. O'Connell *et al.*, *Science* **297**, 593 (2002).
8. M. S. Strano *et al.*, *J. Phys. Chem. B* **107**, 6979 (2003).
9. M. L. Usrey, E. S. Lippmann, M. S. Strano, *J. Am. Chem. Soc.* **127**, 16129 (2005).
10. W. E. Moerner, M. Orrit, *Science* **283**, 1670 (1999).
11. L. Cognet *et al.*, *Sci. STKE* **2006**, pe13 (2006).
12. A. Hartschuh *et al.*, *Science* **301**, 1354 (2003).
13. J. Lefebvre *et al.*, *Phys. Rev. B* **69**, 075403 (2004).
14. D. A. Tsyboulski, S. M. Bachilo, R. B. Weisman, *Nano Lett.* **5**, 975 (2005).
15. See supporting material on *Science* Online.
16. R. M. Dickson *et al.*, *Science* **274**, 966 (1996).
17. S. M. Bachilo *et al.*, *Science* **298**, 2361 (2002).
18. G. Dukovic *et al.*, *J. Am. Chem. Soc.* **126**, 15269 (2004).
19. M. S. Strano *et al.*, *Science* **301**, 1519 (2003).
20. J. L. Bahr *et al.*, *J. Am. Chem. Soc.* **123**, 6536 (2001).
21. C. A. Dyke *et al.*, *Synlett* **2004**, 155 (2004).
22. D. Bonifazi *et al.*, *Nano Lett.* **6**, 1408 (2006).
23. The studied SWNT species were (7,3), (7,5), (7,6), (8,3), (8,6), (9,5), (9,7), (10,5), (12,1), (11,1), and (11,3).
24. A. Hagen *et al.*, *Phys. Rev. Lett.* **95**, 197401 (2005).
25. M. Jones *et al.*, *Nano Lett.* **7**, 300 (2007).
26. C. D. Spataru *et al.*, *Phys. Rev. Lett.* **95**, 247402 (2005).
27. M. S. Dresselhaus, G. Dresselhaus, Ph. Avouris, *Carbon Nanotubes: Synthesis, Structure, Properties, and Applications* (Springer-Verlag, New York, 2001).
28. R. M. Russo *et al.*, *Phys. Rev. B* **74**, 041405 (2006).
29. O. J. Korovyanko *et al.*, *Phys. Rev. Lett.* **92**, 017403 (2004).
30. H. Htoon *et al.*, *Phys. Rev. Lett.* **93**, 027401 (2004).
31. D. A. Heller *et al.*, *J. Am. Chem. Soc.* **126**, 14567 (2004).

32. Supported by the Fulbright Foundation and Delegation Generale pour l'Armement (DGA) grant ERE060016 (L.C.), Welch Foundation postdoctoral fellowship L-C-0004 (D.A.T.), the Rice-Houston Alliances for Graduate Education in the Professoriate (AGEP) program (NSF Cooperative HRD-0450363) (J.D.R.R.), NSF grant CHE-0314270, NSF Center for Biological and Environmental Nanotechnology grant EEC-0647452, Welch Foundation grant C-0807, NASA grant JSC-NNJ06HC25G, and Applied NanoFluorescence LLC. We thank J. T. Willerson, S. W. Casscells III, and J. L. Conyers for instrumentation support.

Supporting Online Material

www.sciencemag.org/cgi/content/full/316/5830/1465/DC1
Materials and Methods
Figs. S1 to S2
Movie S1
References

14 February 2007; accepted 23 April 2007
10.1126/science.1141316

Seismic Evidence for Deep-Water Transportation in the Mantle

Hitoshi Kawakatsu* and Shingo Watada

We report seismic evidence for the transportation of water into the deep mantle in the subduction zone beneath northeastern Japan. Our data indicate that water is released from the hydrated oceanic crust at shallow depths (≲100 kilometers) and then forms a channel of hydrated mantle material on top of the subducting plate that is the pathway for water into the deep mantle. Our result provides direct evidence that shows how water is transported from the ocean to the deep mantle in a cold subduction zone environment.

Water in the mantle is expected to play essential roles in various notable problems of geodynamics, such as the generation of arc volcanism (*1*), lubrication of the subduction zone plate interface that may trigger large earthquakes (*2*), and control of mantle rheology (*3*). How water is transported into the mantle, however, has not been clear, except that it is generally believed that subducting hydrated oceanic crust is the major carrier, preventing Earth scientists from accurately estimating the overall water circulation budget of the Earth system (*4*).

Beneath northeastern Japan, the old Pacific plate is subducting along the Japan trench. Owing partly to the favorable subduction geometry, as well as the dense and well-maintained seismic network there, it is the most detail-studied subduction zone on the planet, and a number of discoveries of subduction processes have been made there. In recent years, these have included the finding of a double seismic zone (*5*); detailed mapping of a low-velocity area in the mantle wedge that possibly corresponds to a pathway of magmatic melt migration responsible for arc volcanism (*6*–*8*); fingerlike distribution of active volcanoes (*9*, *10*); and a transition from the trench-parallel to trench-normal seismic anisotropy (*11*). On the basis of these findings, we now have a much better understanding of the detailed mechanics of subduction. However, if we consider a subduction zone as a place of material consumption (subduction of the oceanic plate)

Earthquake Research Institute, University of Tokyo, 1-1-1 Yayoi, Bunkyo-ku, Tokyo 113-0032, Japan.

*To whom correspondence should be addressed. E-mail: hitosi@eri.u-tokyo.ac.jp

Supporting Online Material for

Stepwise Quenching of Exciton Fluorescence in Carbon Nanotubes by Single-Molecule Reactions

Laurent Cognet,* Dmitri A. Tsyboulski, John-David R. Rocha, Condell D. Doyle, James M. Tour, R. Bruce Weisman*

*To whom correspondence should be addressed. E-mail: lcognet@u-bordeaux1.fr (L.C.); weisman@rice.edu (R.B.W.)

Published 8 June 2007, *Science* **316**, 1465 (2007)
DOI: 10.1126/science.1141316

This PDF file includes:

Material and Methods

Sample preparation

SWNTS were dispersed in 1% aqueous SDBS using a slightly modified version of the protocol introduced by O'Connell et al. (*1*). Very brief (typically 5 s) ultrasonication with a immersion tip probe was used in order to obtain long intact nanotubes (*2*). Then 4% agarose gels prepared with 1% SDBS solution were melted, cooled slowly to 60°C in a water bath, mixed thoroughly with the nanotube suspension, partially sandwiched between a 22×22 mm glass coverslip and a glass slide, and allowed to cool to produce a ~10 μm thick sample. (Fig. S1).

Imaging apparatus

SWNT samples were mounted onto an inverted microscope (Nikon TE-2000U) equipped with a 60× objective (NA = 1.4, Nikon). An additional 1.5× magnification was used such that a single pixel dimension corresponded to 335 nm. Samples were continuously excited from above by a 658 nm diode laser beam. The infrared photoluminescence emitted by the SWNTs passed through long-pass infrared filters (LP950, Thorlabs) and was detected by a liquid nitrogen-cooled 16-bit InGaAs 2D array (OMA-V 2D, Princeton Instruments). Each count corresponds to 3 detected photons, so full scale is ~200,000 detected photons. In this study, typical nanotubes signals are several 10,000 counts/pixel. Luminescence images sequences were recorded with an integration time of 50 ms and a readout dead-time of 4 ms for up to 20,000 consecutive frames. A second port of the microscope was fiber optically coupled to a near-IR spectrograph with multichannel InGaAs detector for recording SWNT emission spectra.

References and Notes

1. M. O'Connell et al., *Science* **297**, 593 (2002).
2. D. A. Tsyboulski, S. M. Bachilo, R. B. Weisman, *Nano Lett.* **5**, 975 (2005).

Figure S1

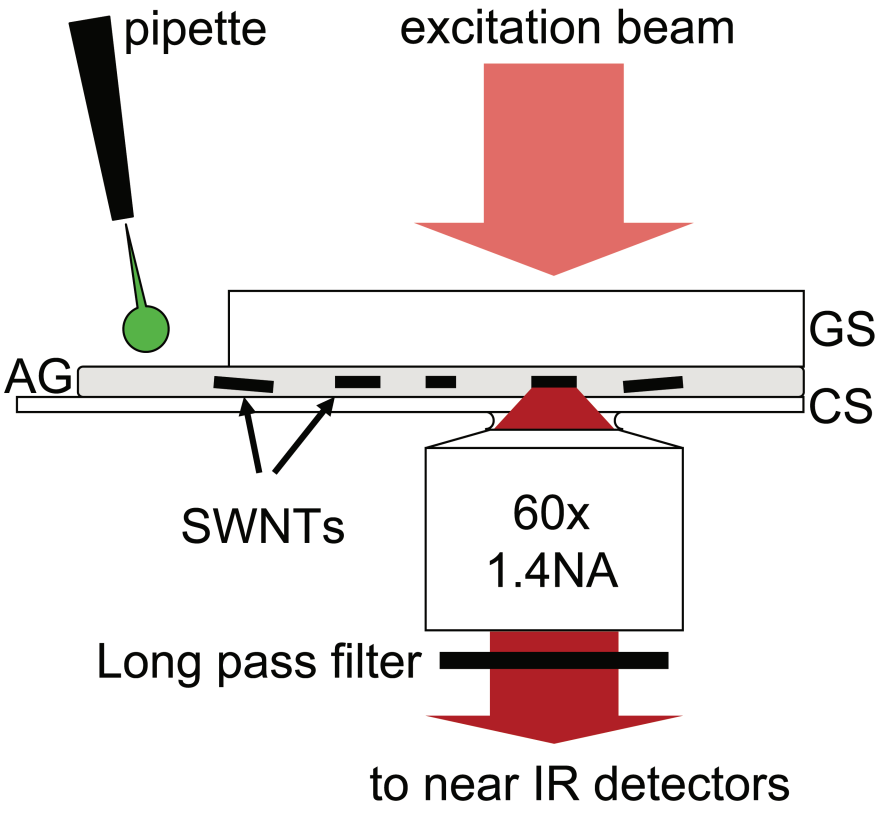
pipette
excitation beam
GS
AG
CS
SWNTs
60x
1.4NA
Long pass filter
to near IR detectors

Figure S2